Ordered Arrays of Dual-Diameter Nanopillars for Maximized Optical Absorption

Zhiyong Fan,[†,‡,§] Rehan Kapadia,[†,‡,§] Paul W. Leu,[†,‡,§] Xiaobo Zhang,[†,‡,§] Yu-Lun Chueh,[†,‡,§] Kuniharu Takei,[†,‡,§] Kyoungsik Yu,[†,§] Arash Jamshidi,[†,§] Asghar A. Rathore,[†,‡,§] Daniel J. Ruebusch,[†,‡,§] Ming Wu,[†,§] and Ali Javey[†,‡,§,*]

[†]Department of Electrical Engineering and Computer Sciences, University of California at Berkeley, Berkeley, California 94720, [‡]Materials Sciences Division, Lawrence Berkeley National Laboratory, Berkeley, California 94720, and [§]Berkeley Sensor and Actuator Center, University of California at Berkeley, Berkeley, California 94720

ABSTRACT Optical properties of highly ordered Ge nanopillar arrays are tuned through shape and geometry control to achieve the optimal absorption efficiency. Increasing the Ge materials filling ratio is shown to increase the reflectance while simultaneously decreasing the transmittance, with the absorbance showing a strong diameter dependency. To enhance the broad band optical absorption efficiency, a novel dual-diameter nanopillar structure is presented, with a small diameter tip for minimal reflectance and a large diameter base for maximal effective absorption coefficient. The enabled single-crystalline absorber material with a thickness of only 2 μm exhibits an impressive absorbance of ~99% over wavelengths, $\lambda = 300-900$ nm. These results enable a viable and convenient route toward shape-controlled nanopillar-based high-performance photonic devices.

KEYWORDS Nanopillar photonics, light management, photovoltaics, light trapping, anti-reflectivity

Due to their one-dimensional geometry, semiconductor nanowires (NWs) have unique optical properties, including polarized photoresponse and diameter tunable band structure.[1−8] Furthermore, engineered three-dimensional (3-D) arrays of NWs and nanopillars (NPLs) enable implementation of novel photon managing (PM) device structures with highly tunable and significantly improved performances.[9−17] Extending on these initial works, here, by using germanium (Ge) as a model material system, optical properties of highly ordered NPL arrays are tuned through shape and geometry control to achieve the optimal broad band absorption. Specifically, a novel dual-diameter NPL (DNPL) structure is presented with a small diameter tip for minimal reflectance and a large diameter base for maximal absorption of the penetrating photons, enabling absorption of ~99% of the incident light over wavelengths, $\lambda = 300-900$ nm with a thickness (DNPL length) of only 2 μm.

Theoretical and experimental works have shown that 3-D arrays of semiconductor NPLs with well-defined diameter, length, and pitch have tunable reflectance, transmittance, and absorption.[12,14,18,19] An optimal combination of dimensions and shape for a given material system leads to maximized broad band light absorption. However, in practice, precise control of these geometric parameters over large scales is rather challenging. One conceivable approach is to utilize lithography to define the precise locations of metal nanoparticles on single-crystalline substrates to initiate

vapor−liquid−solid growth of an epitaxial NPL array.[13,20−22] This approach poses stringent requirements on material and substrate choice, not to mention the complexity and cost of the process. In another approach, Langmuir−Blodgett assembly of micro/nanospheres on a planar substrate followed by chemical etching can enable the fabrication of a micro/nanopillar array.[15,19] However, the single-crystal substrate requirement of this approach poses a limitation in terms of cost and materials choice. Here, we utilize self-organized anodic alumina membranes (AAM) as templates for the VLS growth of ordered, single-crystalline Ge NPL arrays on aluminum foils with controlled shape and dimensions. This process enables fine control over geometry and shape of NPL arrays, without the use of complex epitaxial and/or lithographic processes. Furthermore, since AAM is optically transparent with a wide optical band gap ($E_g = 4.2$ eV),[23] it is an ideal platform for elucidating the intrinsic optical properties of 3-D NPL arrays.

To achieve perfectly hexagonally ordered AAM, a two-step anodization process in conjunction with a simple imprint method was utilized.[11] Electroplating was then performed to deposit Au catalytic seeds selectively at the bottom of each pore followed by the VLS growth of Ge NPLs and ion milling surface cleaning (see Supporting Information). Finally, the Al support substrate was chemically etched and the membrane was attached to a transparent glass handling substrate by epoxy. When the process conditions are tuned, including anodization voltage, time, and nanopore etching time (see Figure S1 in Supporting Information), the dimensions of the pores and the subsequently grown NPLs can be precisely controlled over a wide range. Scanning electron microscopy (SEM) images of AAM before and
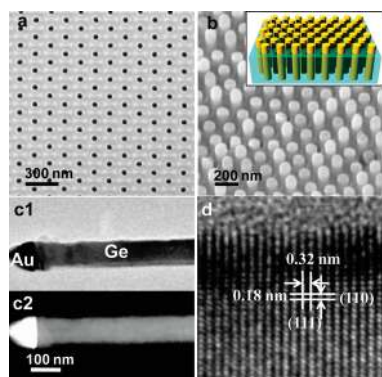
FIGURE 1. Template-assisted VLS growth of ordered Ge NPL arrays. SEM images of a hexagonally ordered AAM (a) before and (b) after the growth of Ge NPLs. The inset in (b) shows the schematic of the enabled structure after Ge NPL growth in AAM and the partial etch of the membrane. (c) Bright field (c1) and high-angle annular dark-field (c2) TEM images of a single Ge NPL terminated with a Au catalytic seed. (d) High-resolution TEM image demonstrates the single crystalline nature of the Ge NPL and [111] growth direction for this particular NPL.

after Ge NPL growth are shown in Figure 1a,b, clearly depicting the large-scale ordering of the NPLs with uniform diameter and pitch. The template-assisted, VLS grown Ge NPLs are single crystalline with preferred growth orientation along [111], as shown in Figure 1c,d, although other orientations also exist (see Figure S2 in Supporting Information).

Optical properties of Ge NPL arrays, including reflectance, transmittance, and absorption, were systematically characterized as a function of NPL diameter, $D_{NPL} = 60-130$ nm, with a fixed pitch of ~150 nm and length of ~2 μm. The 2 μm thickness used in this study presents the characteristic length-scale associated with Ge for achieving significant photon absorption in the visible wavelength range.[24] In order to reduce the parasitic reflectance from alumina membranes, AAMs were partially etched to expose ~100 nm length of Ge NPLs, as shown in Figure 1b. The reflectance spectra of Ge NPL arrays are shown in Figure 2a. As compared to the modeled reflectance of a 2 μm Ge TF (see Figure S3 in Supporting Information), Ge NPL arrays exhibit drastically reduced reflectance. Furthermore, for a constant pitch of 150 nm, a monotonic reduction of reflectance with miniaturization of the diameter is evident (Figure 2a,b). The diameter dependency results may be understood through consideration of the high reflectivity of smooth Ge surfaces due to the relatively high refractive index and the Ge filling ratio (F_R) for a given diameter. In fact, we observe a near-linear F_R dependency of the NPL array reflectance as shown in Figure 2b inset. In our structure

$$F_R = \frac{\pi D_{NPL}^2}{8\sqrt{3}d^2}$$

where d is half of the interpore distance (i.e., pitch) of the AAM. The linear relationship clearly demonstrates that the reflectance from a NPL array is primarily dominated by the effective area of Ge on the top surface.

The transmittance of Ge NPL arrays with different diameters was also characterized. Interestingly, a blue shift in wavelength corresponding to the onset of measurable transmittance is observed as the NPL diameter is reduced. The measured transmittance spectra were well reproduced with simulations using Lumerical Finite Difference Time Domain (FDTD) solution (Version 6.5.9) due to the precisely controlled NPL geometry in the experimental work (see Figure S4 in Supporting Information). To reveal the propagation nature of an EM wave in the Ge NPL array, the simulated cross-sectional electric field intensity $|E|^2$ through the center of a NPL is visualized and shown in the inset of Figure 2c, for $D_{NPL} = 60$ nm (c1) and 100 nm (c2) using 800 nm wavelength incident light. The incident light is normal to the top AAM surface with the electric field polarized so that it is pointing out of the figure. Symmetric and antisymmetric boundary conditions are used appropriately to simulate a periodic structure. The calculations are performed with a grid size of 5 nm ×5 nm ×5 nm. From the simulation, it can be clearly seen that as a subwavelength object, a significant portion of the electromagnetic (EM) wave is propagating outside the NPL as an evanescent wave, showing rapid decay nature in the radial direction. This agrees with other reported works using one-dimensional nanostructures as subwavelength waveguides.[25,26] Electric field intensity $|E|^2$ also decays axially as the EM wave is propagated down into the structure due to the absorption of the photons by Ge NPLs. The transmittance depends on the Ge material filling ratio and optical absorption coefficient α at the wavelength of the incident light. For short wavelengths, $\lambda < \sim500$ nm, minimal transmittance is observed for all NPL diameters with $L \sim 2$ μm due to the high α. On the other hand, for wavelengths near the band gap, where α is moderate, the change in F_R drastically shifts the transmittance spectrum. This characteristic presents a simple route toward realization of optical filters based on engineered NPL arrays.

Acquisition of reflectance (R) and transmittance (T) spectra from Ge NPL arrays allows further obtaining of their absorption (A) spectra, expressed as $A(\%) = 100 - R(\%) - T(\%)$ (Figure 2d). The reflectance measurements do not include diffusely reflected light due to a limitation in the experimental setup. As such, the absorption spectra represent an upper limit. Ge NPL arrays with $D_{NPL} = 130$ nm absorb ~85% of the incident light with minimal wavelength dependence for $\lambda = 300-900$ nm. In this case, the major loss component arises from the surface reflectance (Figure 2a). On the other hand, NPL arrays with $D_{NPL} = 60$ nm show a strong wavelength dependency in the absorption, ranging from ~99% for $\lambda = 300$ nm to ~50% for $\lambda = 900$, arising from their relatively low $F_R \sim 0.14$.

The above results demonstrate the trade-off between reflectance and transmittance for engineered NPL arrays. While it is possible to enhance the broad band optical absorption for smaller NPLs by increasing their length, doing so would be nonoptimal for certain device applications due
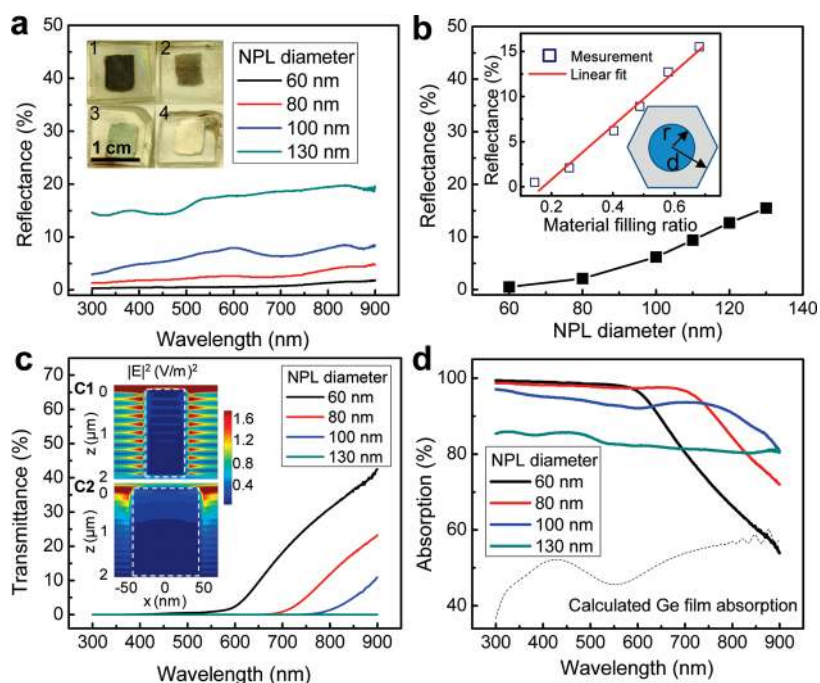
FIGURE 2. Optical characterization of Ge NPL arrays. (a) Experimental reflectance spectra of four Ge NPL arrays with NPL length, $L \sim 2\ \mu m$ and diameters of 60, 80, 100, and 130 nm, corresponding to samples 1−4 shown in the inset, respectively. (b) NPL diameter dependency of the average reflectance as obtained from the spectra shown in (a). The inset shows the reflectance dependence on the material filling ratio, F_R, defined as the occupation of a NPL cross section area in a hexagonal unit cell of AAM. (c) Experimental transmittance spectra of the four samples shown in (a). The insets c1 and c2 are the simulated cross-sectional, electric-field intensity $|E|^2$ distribution for a 800 nm wavelength propagating wave in a Ge NPL with D_{NPL} = 60 and 100 nm, respectively. (d) Absorption spectra obtained from $A\ (\%) = 100 − R\ (\%) − T\ (\%)$ for different diameter NPL arrays. The absorption spectrum of a Ge TF with a 2 μm thickness is obtained from numerical simulation and plotted for comparison.

to the increased parasitic resistances and/or decreased carrier collection efficiency. To address this challenge, here, we introduce a novel shape-controlled NPL structure to achieve the optimal absorption. Figure 3a illustrates a schematic of such a unique structure, composed of Ge NPLs with small diameter (D1 = 60 nm) tip for minimal reflectance and large diameter (D2 = 130 nm) base for enhanced F_R and hence absorption (see Figure S5 in Supporting Information). This DNPL array functions as an efficient broad band optical absorber to achieve high internal quantum efficiency. The tip portion of the DNPL array with small diameter has low reflectance, leading to efficient photon trapping and transmission down to the base. Meanwhile, the base layer with large diameter has high material filling ratio and thus can efficiently absorb the EM wave energy. Figure 3b demonstrates the cross-sectional simulated electric-field intensity ($|E|^2$) distribution of an individual DNPL, which confirms the above rationale.

By utilizing template assisted bottom-up growth, such a DNPL array can be conveniently constructed. Since the diameter of Ge NPLs is controlled by the pore size of the AAM template, the dual-diameter structure can be achieved by using a multistep anodization process at the same voltage, but with a different pore widening etching time for each step (Method section). Figure 3c shows an up-side-down SEM image of a cross-section of a blank AAM (i.e., before growth) with pores composed of two sections with top and bottom

diameters of ∼40 and 110 nm, respectively. After the subsequent VLS growth, highly ordered, Ge DNPLs embedded in the aforementioned AAM with D1 ∼ 60 nm and D2 ∼ 130 nm are formed (Figure 3c, inset). Note that due to the thermal expansion of the Al substrate and AAM during the VLS growth, Ge NPL diameters are typically slightly larger than that of the initial AAM pores. To more clearly depict the structure of Ge DNPLs, the AAM was chemically etched away and individual DNPLs were drop-casted onto a Si substrate for SEM observation (Figure 3d). In addition, transmission electron microscopy (TEM) investigation, shown in Figure 3e, confirms that Ge DNPLs are impressively singlecrystalline with consistent growth orientation along the axis of the entire DNPL, even in the diameter transition region. This is attributed to the fact that the Au catalytic seeds are in the liquid phase during the VLS growth and thus are well confined by the pore boundaries with their diameter being directly controlled by the pore diameter. This presents a unique approach for shape controlled synthesis of singlecrystalline nanostructures for desired functionality—an important aspect for practical applications.

DNPL arrays exhibit unique PM properties. The experimental absorption spectra of a Ge DNPL array, with D1 = 60 nm and D2 = 130 nm and equal lengths of 1 μm for the two segments (total length of 2 μm), together with singlediameter NPL arrays with D_{NPL} = 60 and 130 nm are plotted in Figure 4a. The Ge DNPL array exhibits 95−100% absorp-
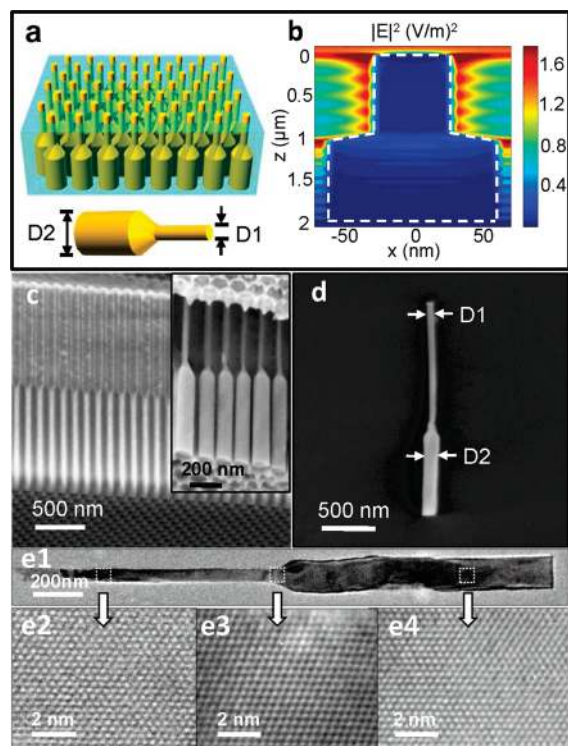
FIGURE 3. Ge dual-diameter nanopillar arrays. (a) Schematic of a DNPL array embedded in AAM. (b) Simulated cross-sectional electric-field intensity distribution for a 800 nm wavelength EM wave propagating in a DNPL with a tip diameter $D1 = 60$ nm and a base diameter $D2 = 130$ nm. (c) Cross-sectional SEM images of a blank AAM with dual-diameter pores and the Ge DNPLs (inset) after the growth. (d) SEM of a single Ge DNPL after harvesting and drop-casting on a silicon substrate. (e1−e4) TEM images of a Ge DNPL, showing the single-crystalline structure along its axis.

FIGURE 4. Optical characterization of Ge DNPL array. (a) Experimental absorption spectra of a DNPL array with $D1 = 60$ nm and $D2 = 130$ nm, and single-diameter NPL arrays with diameters of 60 and 130 nm. (b) Average absorption efficiency over $\lambda = 300-900$ nm for single-diameter NPLs as a function of diameter along with that of a DNPL array with $D1 = 60$ nm and $D2 = 130$ nm.

tion for $\lambda = 900-300$ nm, which is a drastic improvement over single-diameter NPLs (Figure 4a). The broad band absorption enhancement for the DNPL geometry is depicted in Figure 4b, where the average absorption efficiency, $\bar{A}$, for $\lambda = 900-300$ nm is plotted for various Ge planar and nanopillar structures. For single-diameter NPLs, a strong diameter dependency is observed, with a peak $\bar{A} \sim 94\%$, corresponding to $D_{NPL} = 80$ nm. A drop in $\bar{A}$ is observed for the smaller and larger NPLs due to reduced F_R and enhanced R, respectively, as previously explained. On the other hand, DNPLs with $D1 = 60$ nm and $D2 = 130$ nm exhibit $\bar{A} \sim 99\%$, clearly demonstrating the advantage of this novel structure for near unity absorption in the explored wavelength range. Notably, both NPL and DNPL structures drastically outperform planar Ge TFs, where $\bar{A} \sim 53\%$, despite using significantly less material ($F_R = 0.2-0.6$) and clearly proving their superiority in PM properties.

In summary, a versatile approach for controlled synthesis of ordered nanopillar arrays with tunable shape and diameter is presented, enabling a systematic study of the intrinsic optical properties of 3-D NPL structures. Specifically, Ge DNPL arrays are demonstrated as a novel platform for decoupling reflectance from transmittance, therefore, enabling maxim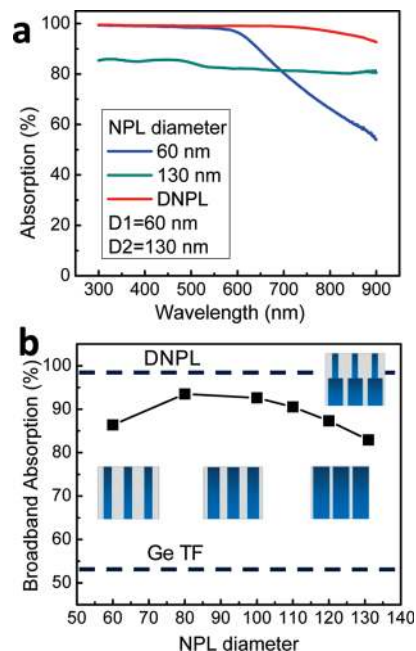al broad band photon absorption, optimal for potential photovoltaic and/or broad band detector applications. In this work, the effects of varying pitch on light absorption were not explored. In the future, pitch optimization can be used to enable light trapping and hence significant absorption enhancement with smaller F_R. Furthermore, the DNPL structure may enable the exploration of novel photonic devices. Here, the diameter of the explored NPLs is larger than the Bohr radius of Ge ($R_B = 24.3$ nm);[27] therefore quantum confinement does not play a role. In the future, templates with pore diameters $<R_B$ can be utilized for band-structure engineering of Ge NPLs, providing another degree of control over the absorption properties of NPL arrays. For instance, a tandem cell can be envisioned based on a single material system by appropriate diameter selection of the two segments of the DNPL structure, further enhancing the utility of the proposed approach. While we focused on Ge as a model system, the approach is highly generic for various semiconductors and, in the future, can be applied to the application specific material system.

Supporting Information Available. Details of the AAM fabrication process and Ge NPL growth; TEM studies of

NANO LETTERS

Ge NPLs; simulation of reflectance, transmittance, and absorption spectra of Ge TF and NPL arrays; and optical photographs of Ge NPL samples. This material is available free of charge via the Internet at http://pubs.acs.org.

REFERENCES AND NOTES

(1) Wang, J. F.; Gudiksen, M. S.; Duan, X. F.; Cui, Y.; Lieber, C. M. *Science* **2001**, *293*, 1455–1457.

(2) Fan, Z. Y.; Chang, P. C.; Lu, J. G.; Walter, E. C.; Penner, R. M.; Lin, C. H.; Lee, H. P. *Appl. Phys. Lett.* **2004**, *85*, 6128–6130.

(3) Fan, Z. Y.; Ho, J. C.; Jacobson, Z. A.; Razavi, H.; Javey, A. *Proc. Natl. Acad. Sci. U.S.A.* **2008**, *105*, 11066–11070.

(4) Yan, R.; Gargas, D.; Yang, P. D. *Nat. Photonics* **2009**, *3*, 569–576.

(5) Lieber, C. M.; Wang, Z. L. *MRS Bull.* **2007**, *32*, 99–104.

(6) Gudiksen, M. S.; Wang, J.; Lieber, C. M. *J. Phys. Chem. B* **2002**, *106*, 4036–4039.

(7) Javey, A. *ACS Nano* **2008**, *2*, 1329–1335.

(8) Tian, B. Z.; Zheng, X. L.; Kempa, T. J.; Fang, Y.; Yu, N. F.; Yu, G. H.; Huang, J. L.; Lieber, C. M. *Nature* **2007**, *449*, 885–889.

(9) Cao, L. Y.; Fan, P. Y.; Vasudev, A. P.; White, J. S.; Yu, Z. F.; Cai, W. S.; Schuller, J. A.; Fan, S. H.; Brongersma, M. L. *Nano Lett.* **2010**, *10*, 439–445.

(10) Chueh, Y. L.; Fan, Z. Y.; Takei, K.; Ko, H.; Kapadia, R.; Rathore, A. A.; Miller, N.; Yu, K.; Wu, M.; Haller, E. E.; Javey, A. *Nano Lett.* **2010**, *10*, 520–523.

(11) Fan, Z. Y.; Razavi, H.; Do, J. W.; Moriwaki, A.; Ergen, O.; Chueh, Y. L.; Leu, P. W.; Ho, J. C.; Takahashi, T.; Reichertz, L. A.; Neale, S.; Yu, K.; Wu, M.; Ager, J. W.; Javey, A. *Nat. Mater.* **2009**, *8*, 648–653.

(12) Hu, L.; Chen, G. *Nano Lett.* **2007**, *7*, 3249–3252.

(13) Boettcher, S. W.; Spurgeon, J. M.; Putnam, M. C.; Warren, E. L.; Turner-Evans, D. B.; Kelzenberg, M. D.; Maiolo, J. R.; Atwater, H. A.; Lewis, N. S. *Science* **2010**, *327*, 185–187.

(14) Kelzenberg, M. D.; Boettcher, S. W.; Petykiewicz, J. A.; Turner-Evans, D. B.; Putnam, M. C.; Warren, E. L.; Spurgeon, J. M.; Briggs, R. M.; Lewis, N. S.; Atwater, H. A. *Nat. Mater.* **2010**, Advanced Online Publication.

(15) Garnett, E. C.; Yang, P. D. *Nano Lett.* **2010**, *10*, 1082–1087.

(16) Garnett, E. C.; Yang, P. D. *J. Am. Chem. Soc.* **2008**, *130*, 9224–9225.

(17) Spurgeon, J. M.; Atwater, H. A.; Lewis, N. S. *J. Phys. Chem. C* **2008**, *112*, 6186–6193.

(18) Lin, C. X.; Povinelli, M. L. *Opt. Express* **2009**, *17*, 19371–19381.

(19) Zhu, J.; Yu, Z. F.; Burkhard, G. F.; Hsu, C. M.; Connor, S. T.; Xu, Y. Q.; Wang, Q.; McGehee, M.; Fan, S. H.; Cui, Y. *Nano Lett.* **2009**, *9*, 279–282.

(20) Borgstrom, M. T.; Immink, G.; Ketelaars, B.; Algra, R.; Bakkers, E. P. A. M. *Nat. Nanotechnol.* **2007**, *2*, 541–544.

(21) Martensson, T.; Carlberg, P.; Borgstrom, M.; Montelius, L.; Seifert, W.; Samuelson, L *Nano Lett.* **2004**, *4*, 699–702.

(22) Martensson, T.; Borgstrom, M.; Seifert, W.; Ohlsson, B. J.; Samuelson, L. *Nanotechnology* **2003**, *14*, 1255–1258.

(23) Wang, J.; Wang, C. W.; Li, Y.; Liu, W. M. *Thin Solid Films* **2008**, *516*, 7689–7694.

(24) Nelson, J. *The physics of solar cells*; Imperial College Press: London, 2003.

(25) Sirbuly, D. J.; Tao, A.; Law, M.; Fan, R.; Yang, P. D. *Mater.* **2007**, *19*, 61–66.

(26) Sirbuly, D. J.; Law, M.; Yan, H. Q.; Yang, P. D. *J. Phys. Chem. B* **2005**, *109*, 15190–15213.

(27) Gu, G.; Burghard, M.; Kim, G. T.; Dusberg, G. M.; Chiu, P. W.; Krstic, V.; Roth, S.; Han, W. Q. *J. Appl. Phys.* **2001**, *90*, 5747–5751.